PROPAGATION OF A SUBMERGED JET IN A NARROW SLIT

V. D. Zhak, V. A. Mukhin,
V. E. Nakoryakov, and S. A. Safonov

UDC 532.525.2:532.032

The Haley—Shaw apparatus, designed for study of the character of a potential flow over bodies of various form, is a well-known experimental device [1]. It is widely used for simulation of filtration processes in motion with and without a pressure head [2]. The flow in mixing zones at high velocity in such equipment has been studied only in [3, 4], where, unfortunately, very interesting features observed for the first time were not interpreted properly. The present study will offer results of a theoretical and experimental investigation of a laminar jet flow in a narrow slit, together with some experimental data on turbulent jet flow.

We will consider a jet exiting from a plane nozzle of width d = 2r >> h into a submerged slit. The thicknesses of nozzle and slit are identical. The configuration of the flow region to be studied is shown in Fig. 1.

The basic equations of motion for the three-dimensional case have the form

$$\begin{gathered}
u\frac{\partial u}{\partial x}+v\frac{\partial u}{\partial y}+w\frac{\partial u}{\partial z}=-\frac{1}{\rho}\frac{\partial p}{\partial x}-\nu\left(\frac{\partial^2 u}{dx^2}+\frac{\partial^2 u}{\partial y^2}+\frac{\partial^2 u}{\partial z^2}\right),\\
u\frac{\partial v}{\partial x}+v\frac{\partial v}{\partial y}+w\frac{\partial v}{\partial z}=-\frac{1}{\rho}\frac{\partial p}{\partial y}+\nu\left(\frac{\partial^2 v}{\partial x^2}+\frac{\partial^2 v}{\partial y^2}+\frac{\partial^2 v}{\partial z^2}\right),\\
u\frac{\partial w}{\partial x}+v\frac{\partial w}{\partial y}+w\frac{\partial w}{\partial z}=-\frac{1}{\rho}\frac{\partial p}{\partial z}+\nu\left(\frac{\partial^2 w}{\partial x^2}+\frac{\partial^2 w}{\partial y^2}+\frac{\partial^2 w}{\partial z^2}\right),\\
\partial u/\partial x+\partial v/\partial y+\partial w/\partial z=0.
\end{gathered}\tag{1}$$

In the narrow slit, due to the small transverse dimension, the equations may be simplified significantly:

$$\begin{gathered}
u\frac{\partial u}{\partial x}+v\frac{\partial u}{\partial y}=-\frac{1}{\rho}\frac{\partial p}{\partial x}+\nu\left(\frac{\partial^2 u}{\partial x^2}+\frac{\partial^2 u}{\partial y^2}+\frac{\partial^2 u}{\partial z^2}\right),\\
u\frac{\partial v}{\partial x}+v\frac{\partial v}{\partial y}=-\frac{1}{\rho}\frac{\partial p}{\partial y}+\nu\left(\frac{\partial^2 v}{\partial x^2}+\frac{\partial^2 v}{\partial y^2}+\frac{\partial^2 v}{\partial z^2}\right),\\
\partial u/\partial x+\partial v/\partial y=0.
\end{gathered}\tag{2}$$

We will assume that in each section of the slit a Poiseuille profile is locally realized for each velocity component:

$$\begin{aligned}
u&=u_m(x,\ y)(1-4z^2/h^2)=u_m(x,\ y)f(z),\\
v&=v_m(x,\ y)(1-4z^2/h^2)=v_m(x,\ y)f(z).
\end{aligned}\tag{3}$$

Substituting Eq. (3) in Eq. (2), after integration over z from z = —h/2 to z = h/2, we obtain

$$\begin{gathered}
u_m\frac{\partial u_m}{\partial x}+v_m\frac{\partial u_m}{\partial y}=-\frac{15}{8}\frac{1}{\rho}\frac{\partial p}{\partial x}+\frac{5}{4}\nu\Delta u_m-15\frac{\nu}{h^2}u_m,\\
u_m\frac{\partial v_m}{\partial x}+v_m\frac{\partial v_m}{\partial y}=-\frac{15}{8}\frac{1}{\rho}\frac{\partial p}{\partial y}+\frac{5}{4}\nu\Delta v_m-15\frac{\nu}{h^2}v_m,\\
\partial u_m/\partial x+\partial v_m/\partial y=0.
\end{gathered}\tag{4}$$

The system of equations (4), describing the motion of the liquid in the slit, corresponds to the Rakhmatulin—Nigmatulin equation [5, 6] for the motion of multiphase media with a standing dispersed phase. If the inertial and viscous terms are neglected, we obtain the Haley—

Novosibirsk. Translated from Zhurnal Prikladnoi Mekhaniki i Tekhnicheskoi Fiziki, No. 3, pp. 69-77, May-June, 1985. Original article submitted April 27, 1984.

0021-8944/85/2603-0363$09.50 © 1985 Plenum Publishing Corporation

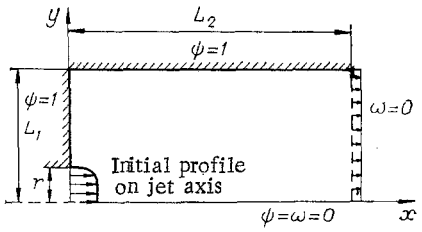

Fig. 1

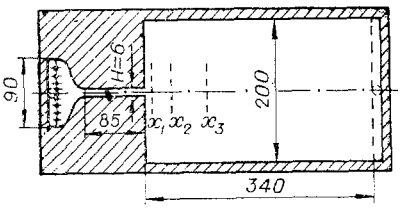

Fig. 2

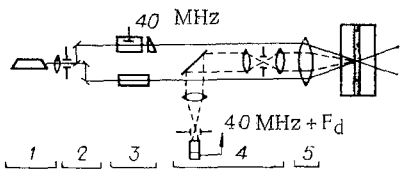

Fig. 3

Shaw flow equation, which coincides with the equations of filtration theory. Consideration of the viscous terms with neglect of the inertial ones gives the Brinkman equation [7].

Numerical solution of the problem of the laminar jet was performed using system (4), written in the variables flow function—vorticity:

$$\frac{\partial\bar{\psi}}{\partial\tilde{y}}\frac{\partial\bar{\omega}}{\partial\tilde{x}}-\frac{\partial\bar{\psi}}{\partial\tilde{x}}\frac{\partial\bar{\omega}}{\partial\tilde{y}}=\frac{5}{3}\frac{1}{\mathrm{Re}}\left(\frac{\Delta\bar{\omega}}{r/h}-12\frac{r}{h}\bar{\omega}\right),\quad \Delta\bar{\psi}=\bar{\omega}, \tag{5}$$

where

$$\bar{\psi}=\frac{\psi}{1{,}5\bar{u}r};\quad \bar{\omega}=\frac{\omega}{1{,}5\bar{u}/r};\quad \mathrm{Re}=\frac{\bar{u}2h}{\nu};\quad \tilde{x}=\frac{x}{r};\quad \tilde{y}=\frac{y}{r}.$$

Boundary conditions at the nozzle exit are specified in accordance with the solution of system (4) neglecting convective terms (stabilized flow). The boundary conditions for ψ and ω on the righthand boundary of the calculation region corresponded to a uniform longitudinal velocity profile; on the axis of symmetry $\psi = \omega = 0$, while on the wall $\psi = 1$, and ω is defined by the Woods condition [8] with the explicit technique of [9].

Calculations were performed using the "upwind" technique of [9] on decreasing size-nonuniform 10 × 10, 19 × 19, 37 × 37 grids with intermediate interpolation.

In the jet portion of the flow the relative changes in velocity values on the jet axis upon the first decrease in grid size comprised 20-40%, with 3-7% (depending on Re) change upon subsequent reduction. To satisfy the conditions $\max(\omega_{ij}^{n+}-\omega_{ij}^{n})<5\cdot10^{-5}\max(\omega_{ij}^{n})$ (where n is the number of iterations) about 2 h of M 4030 processor time was required.

For laminar flow good results were obtained by introducing a colorant liquid into the flow. The colored liquid was introduced through an orifice in the channel wall in the input confusor section of the nozzle (Fig. 2), eliminating the distorting effect of colorant jets on the main flow in the slit. Using this visualization method it was possible to obtain flow line patterns over practically the entire slit field up to Re = 4700.

Experimental studies of velocity fields in the slit were performed with a TSI system 9100-8 laser-Doppler velocity meter. Velocity measurements and flow pattern visualization were done with identical models (see Fig. 2). The slit width h = 0.625 mm. The experimental model was installed in a circuit with a constant level reservoir. The working liquid used was distilled water with silicon carbide powder added (particle size 1.5 μm) to provide scattering particles. The liquid temperature in the channel was maintained constant (to ±0.1°C). Liquid flow rate was measured by a rotameter located at the working section exit. The entire inner section (see Fig. 2) was made of sheet plastic 0.625 mm thick and located between two 24-mm-thick Plexiglas plates. Grooves (14 mm deep, 10 mm wide) were made in the Plexiglas plates to introduce and exhaust liquid to and from the working section. The length of the grooves at the input was equal to the confusor width (90 mm), and to the slit width at the output (200 mm). These grooves formed input and output collectors which insured uniform velocity distributions over the width of the input confusor and at the output from the slit. The nozzle length was 85 mm (L/2h = 70), permitting production of a stabilized flow at the output from the nozzle up to Re ≈ 7000. The experimental section was installed on a coordinate table which allowed displacement over three coordinates to an accuracy of the order of 0.1 mm. The measurement system is shown in Fig. 3, where 1 indicates the laser with collimator; 2, splitter lens; 3, shear cell, with dashed lines indicating detector optics. Focusing lens 5 with focal length of 121.4 mm created a measurement volume 0.35 mm in length at the crossing of the rays. To decrease the length of the measurement volume a ray expander was installed between the detector optics 4 and the focusing lens, producing a reduction in the length of the measurement volume, which comprised 150 μm in the present experiments. Liq-

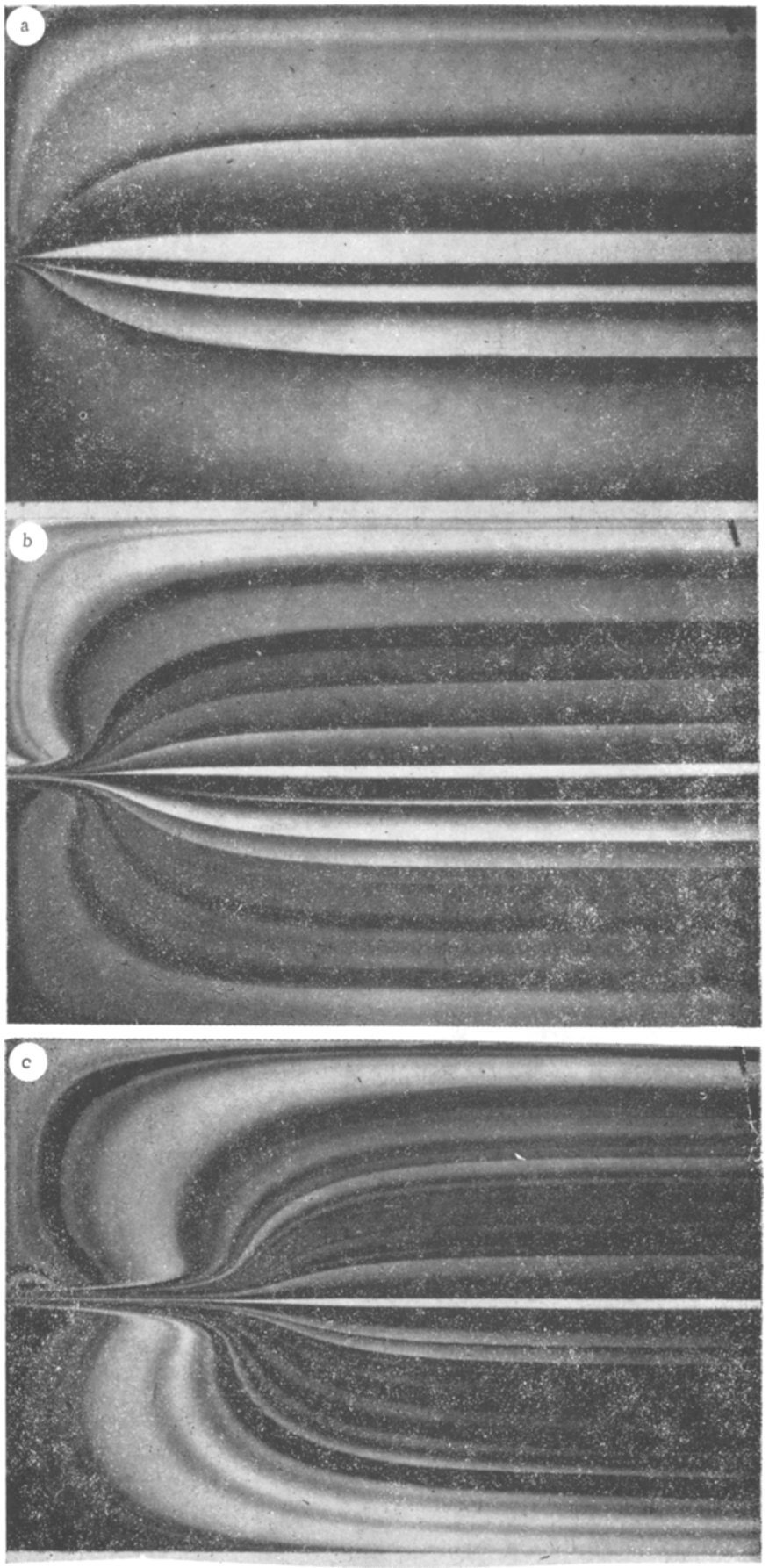

Fig. 4

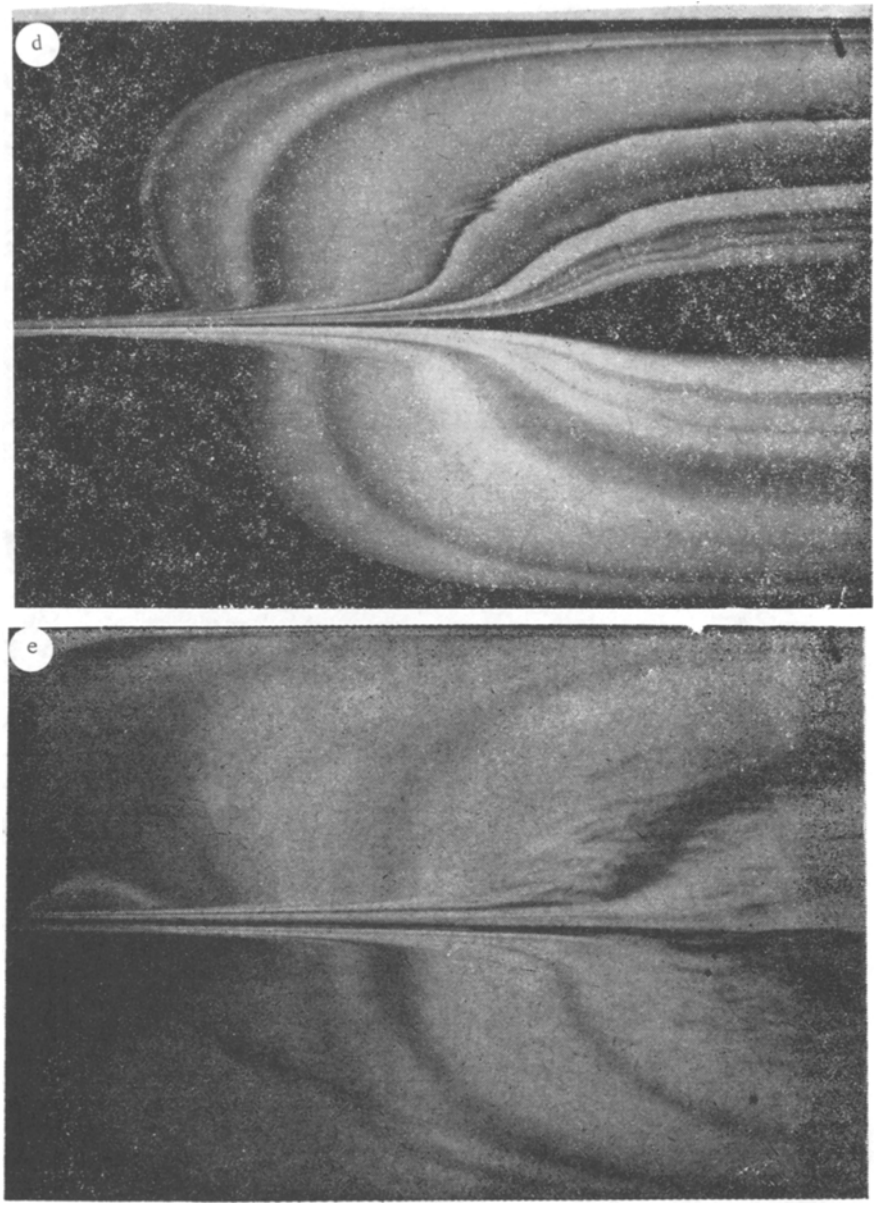

Fig. 4 (Cont'd.)

uid velocity measurements were performed only in the central plane of the slit. Estimates were made of the uncertainty in the velocity measurements caused by the finite size of the measurement volume, assuming that in each section of the slit the velocity profile was parabolic in the transverse direction (Poiseuille profile). Such an estimate gives a maximum error value for the velocity profiles of the order of 6%.

The Doppler signal from the photomultiplier output was fed to a mixer followed by an electronic counter (model 1980), where the Doppler frequency was processed by normal methods. The digital output of the counter was connected to an Apple 6200 computer, to which the mixer frequency, optical system parameters, number of Doppler cycles to be processed, number of samples, and intersample time (0.02 and 0.01 sec) were input from the keyboard.

Results of flow structure studied by visualization of the flow using colored liquid with the model shown in Fig. 2 are presented in Fig. 4, while Fig. 5 shows results of calculation performed with system (5) for the same conditions as the flow visualization experiments [a) Re = 300; b) Re = 1000; c) Re = 2000; d) Re = 3300; e) Re = 4700]. It is quite evident that the flow in the narrow slit formed upon exit of the jet into the submerged space is divided into two portions: a region of jet flow and a region of low-velocity flow. Points at which the flow lines deviate from the original rectilinear segments outline the jet flow region. The agreement between calculation and experiment is qualitatively satisfactory up to Re $\simeq$ 2000. At large Re this agreement is degraded, and the photographs clearly show turbulent perturba-

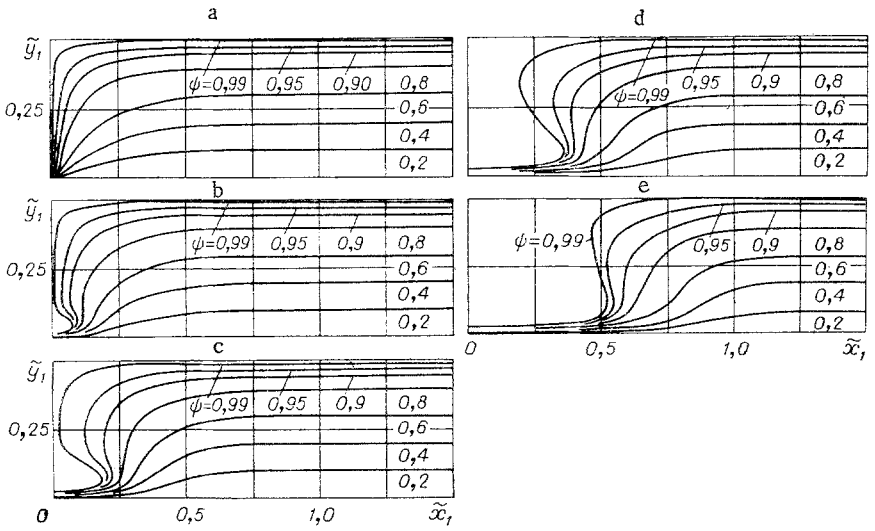

Fig. 5

tions being formed near the axis and propagating down the flow. The Re ≈ 4700 coarse scale turbulent formations are visible in the flow. The intensity of the perturbations decreases with removal (along both x and y) from the point of their formation. With further increase in Re there is an abrupt change in the flow structure: The flow becomes clearly turbulent; the colored liquid tracks diffuse, and the flow becomes invisible. As was indicated above, studies of jet flow in slits have revealed a characteristic feature: an abrupt curvature of the flow lines, which indicates a transition from jet flow, in which a significant role is played by inertial forces, to low-velocity flow. This is caused by the interaction of pressure and friction forces. The abrupt curvature of the flow lines in the "planar" jet flow (we speak of the jet formed in the space between two closely spaced plane plates) is caused by the intense effect of friction on the channel side walls.

The visualization also shows that at the beginning of the working section a low velocity region is formed ("stagnant" zone), which lies directly adjacent to the channel lateral line and the high velocity jet flow directed along the axis. Motion in this region can occur in the direction opposite to that of the main flow. With increase in Re the main flow in the slit as it were moves away from the initial section, the dimensions of the "stagnant" zone increasing.

At the nozzle mouth a closed turbulent region is formed (forming at Re = 1000), the dimensions of which increase with increase in Re. The calculations reflect the real flow pattern well; however, the flowline structure in the stagnant zone could not be obtained because of limited calculation accuracy.

Figures 6-9 show results of measurements of longitudinal velocity component, mean velocity pulsation, and degree of turbulence, obtained with the laser Doppler velocity meter for the same Re values as the flow visualizations. In Figs. 6-9 we introduce the notation:

$$\tilde{x} = x/2r;\ \tilde{u} = u/\bar{u}_1;\ \tilde{u'} = u'/\bar{u}_1;\ \varepsilon = u'/u;$$

$\bar{u}_1$ is the mean flow velocity at the nozzle exit; u', mean square velocity pulsation; u, current mean velocity. In Fig. 6: a) Re = 130; b) Re = 300; c) Re = 1000; d) Re = 2000; e) Re = 3300; f) Re = 4700; a-e) 1, $\tilde{x}$ = 1.7, 2, $\tilde{x}$ = 6.7, 3, $\tilde{x}$ = 15; f) 1, $\tilde{x}$ = 1.2, 2, $\tilde{x}$ = 6.7, 3, $\tilde{x}$ = 12.5; solid lines, calculation; dashes, experiment. In Fig. 7: 1) Re = 1000; 2) Re = 2000; 3) Re = 3300; 4) Re = 4700; 5) Re = 7300; $\tilde{x}$ = 3.33. In Fig. 8: 1) $\tilde{u}$; 2) ε, 3) $\tilde{u}'$, Re = 4700, $\tilde{y}$ = 0. In Fig. 9: 1-6) experiment; 7-12) calculation with Eq. (5); 13-18) calculation with Eq. (6); 1, 7, 13) Re = 130; 2, 8, 14) Re = 300, 3, 9, 15) Re = 1000; 4, 10, 16) Re = 2000; 5, 11, 17) Re = 3300; 6, 12, 18) Re = 4700; $\tilde{y}$ = 0.

Figure 10 shows the change in relative velocity on the nozzle axis (at a distance of 1.5 mm up the flow from the output) as a function of Re. It is evident that up to Re = 10^3 u_1 = 1.5$\bar{u}$, which corresponds to laminar flow between two parallel plates. If we consider that the nozzle cross-sectional dimensions are 6 × 0.625 mm, then according to [10] for stabilized flow in the channel we should obtain a value 1.07 times larger. However, considering the limited accuracy of the measurements (±5%) such agreement can be considered satisfactory. It is evident from Fig. 10 that at Re = 1000 the velocity profile in the nozzle output sec-

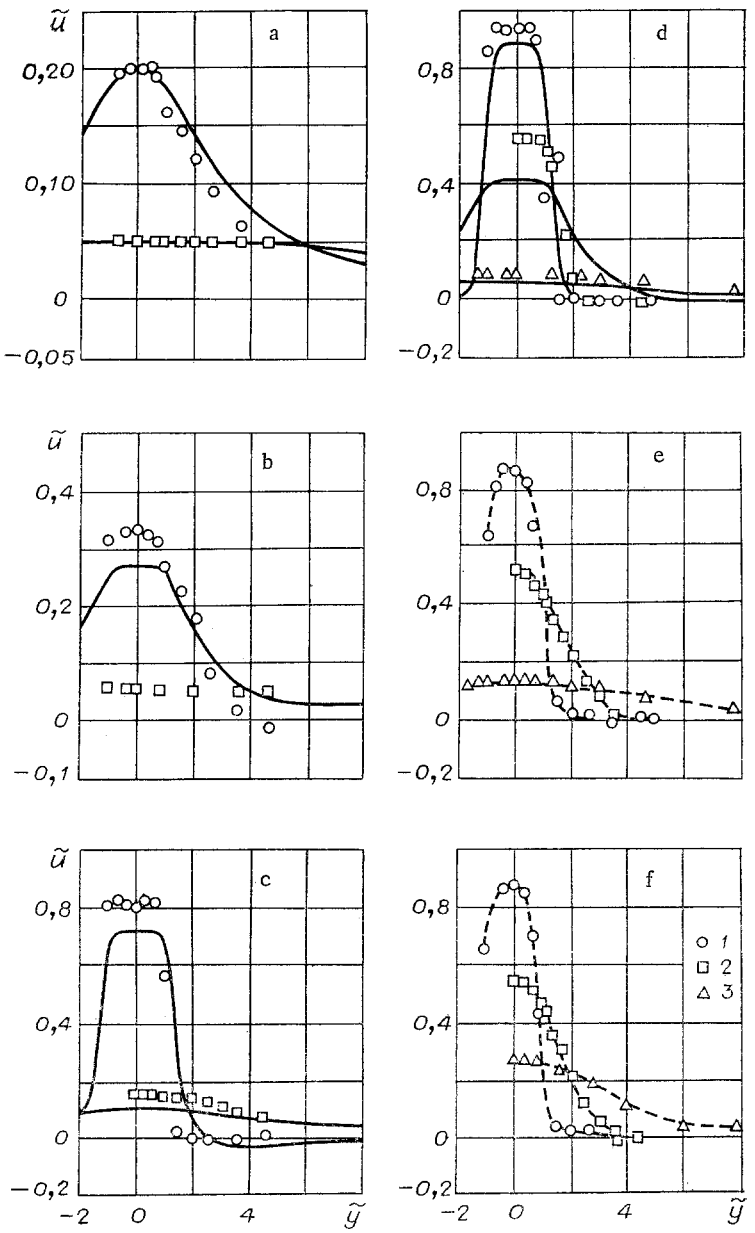

Fig. 6

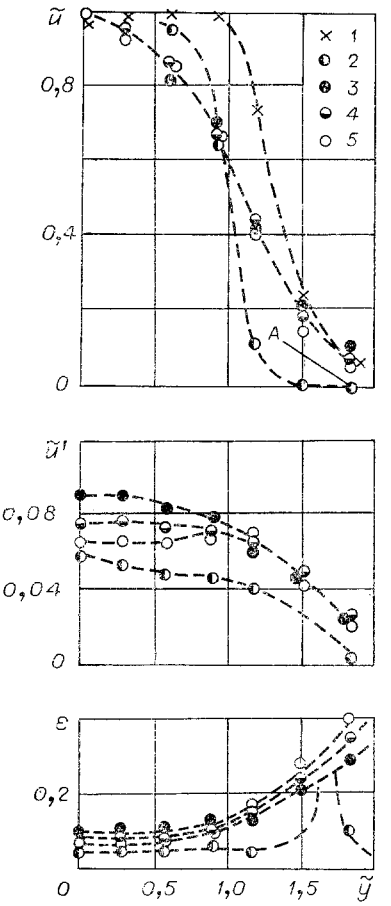

Fig. 7

tion becomes ever more filled, which indicates a transition from laminar to turbulent flow regimes.

We will consider the change in the longitudinal velocity component along x and y for various Re. It is evident that there are sections on the velocity distribution curves along the y axis near the x axis where the longitudinal velocity component is constant, which indicates the presence of a unique "initial section." Within the limits of this initial section, in contrast to the initial section of a conventional jet, the velocity along the x axis decreases. The length of the initial section increases with increase in Re.

The velocity distribution along the jet axis (along x) and along the y axis (for various x values) at Re = 130 and 300 agrees satisfactorily with numerical calculations performed with Eq. (5). From comparison of the experimental data and calculations it is evident that at Re = 10^3 there is some divergence (the experimental data are somewhat higher) with this divergence increasing with increase in Re. Possibly the cause of this should be sought in deviations of the local velocity profiles from a parabolic law.

With further increase in the velocity of the motion (Re $\geqslant$ 2000) turbulent effects begin to be significant. In the transient flow regimes relative velocity pulsations develop (relative to the current velocity value on the axis). The maximum value of these relative pulsations occurs on the jet axis. Beginning at Re = 3300 and above the relative velocity

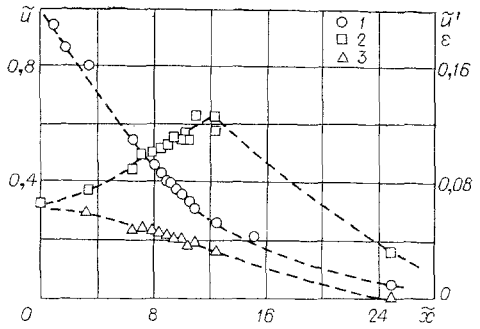

Fig. 8

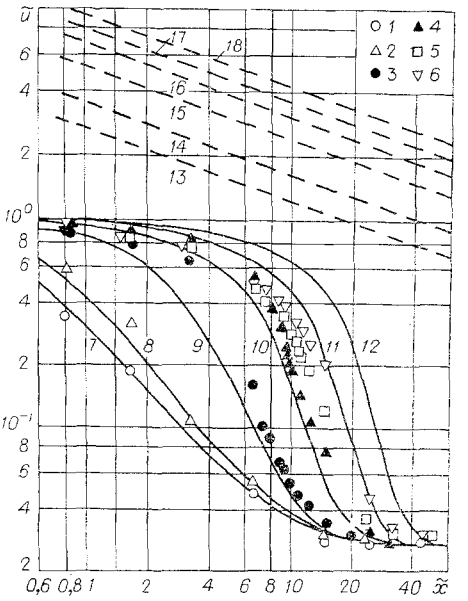

Fig. 9

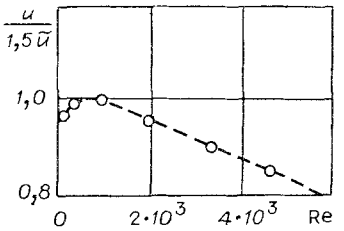

Fig. 10

distributions across the jet (along y) practically coincide with each other. The same may be said of the relative velocity distribution along the x axis.

At Re = 7300 the relative velocity pulsation profile across the jet changes form, with maximum pulsation values occurring at the point corresponding to the inflection point of the velocity profile (along the y axis), as occurs in a conventional turbulent jet. The magnitude of the longitudinal velocity component pulsations then proves to be 2.5 times lower than in a conventional jet, and corresponds approximately to the value of velocity pulsations on the axis of a channel of rectangular section. In the transient and turbulent (Re $\geqslant$ 3300) flow regimes friction on the channel walls increases abruptly, and naturally the velocity values then lie well below calculations for a laminar flow regime. In the upper portion of Fig. 9, which shows velocity distributions along the x axis (for various Re), the dash-dot lines were obtained by calculation with the Schlichting–Bickley formula:

$$\tilde{u} = (0.4543/u_1)(K^2/\nu x). \qquad (6)$$

The calculations were performed for the condition of equality of the initial momentum of the plane jet to the initial momentum of the jet propagating in the narrow slit. Naturally, such a comparison is arbitrary in nature, demonstrating only the difference in laws of velocity change along the jet axis. In Fig. 8, together with the change in longitudinal velocity component, the change in relative pulsations of the longitudinal component and the degree of turbulence along the jet axis are also shown. It is evident that the magnitude of relative pulsations decreases with removal from the nozzle section and the jet axis (Fig. 7), the degree of turbulence initially increases, reaches a maximum, and then decreases to a value significantly below the original one (in the nozzle section). Thus, with decrease in velocity (along x and y) laminarization of the flow occurs. The high stability of the jet flow in the slit should be noted. It is well known that in a conventional planar jet even at Re = 60 the flow becomes unstable and a transition to turbulent flow occurs. A jet propagating in a narrow slit maintains stability up to Re = 2000 (we recall that Re is calculated from the mean flow velocity at the nozzle output and the width of the slit doubled).

LITERATURE CITED

1. H. Schlichting, Boundary Layer Theory, 6th ed., McGraw-Hill (1968).
2. J. Bear, D. Zaslawsky, and S. Irmey, Physico-Mathematical Fundamentals of Water Filtration [Russian translation], Mir, Moscow (1971).
3. Yu. M. Bychkov, Visualization of Thin Flows of Incompressible Liquids [in Russian], Shtiintsa, Kishinev (1980).
4. Yu. M. Bychkov, Hydrodynamics of Thin Flows of Incompressible Liquids [in Russian], Shtiintsa, Kishinev (1981).
5. Kh. A. Rakhmatulin, "Fundamentals of gasdynamics of interpenetrating flows of compressible media," Prikl. Mat. Mekh., 20, No. 2 (1956).
6. R. I. Nigmatulin, Fundamentals of the Mechanics of Heterogeneous Media [in Russian], Nauka, Moscow (1978).
7. N. C. Brinkman, "A calculation of the viscous force exerted by flowing fluid on a dense swarm of particles," Appl. Sci. Res., A1, No. 1 (1949).
8. P. Roach, Computational Hydrodynamics [Russian translation], Mir, Moscow (1980).
9. A. D. Gosmen, V. M. Pan, A. K. Ranchel, et al., Numerical Methods for Study of Viscous Liquid Flows [Russian translation], Mir, Moscow (1972).
10. B. S. Petukhov, Heat Exchange and Resistance in Laminar Fluid Flow in Tubes [in Russian], Énergiya, Moscow (1967).

EFFECT OF VISCOSITY AND HEAT CONDUCTION ON THE ASCENT OF A THERMAL UNDER THE INFLUENCE OF BUOYANCY

N. A. Kudryashov and V. M. Prostokishin

UDC 532.517.4

The ascent of a heated mass of air (thermal) in the earth's atmosphere under the influence of buoyancy is a classical problem [1]. The study [2] examined the motion of a vortex ring without consideration of its internal structure. The approximation yielded basic integral characteristics describing the evolution of a rising cloud. The motion of a heated air mass in the atmosphere was analyzed in [3] without consideration of viscosity and heat conduction. The investigations [4-7] studied convective motion of a thermal on the basis of numerical solution of two-dimensional Navier–Stokes equations with constant values of the viscosity coefficient and thermal conductivity. The present study shows how the temperature dependence of the viscosity coefficient and thermal conductivity affect the ascent of a cloud of heated gas under the influence of buoyancy.

Let a spherical region D_0 of heated gas of radius R_0 be located at the altitude H_0 in the earth's atmosphere at the initial moment of time. The gas has been heated to the temperature $T_1 > T_0$ (T_0 is the temperature of the undisturbed air). The gas pressure inside the spherical region will be assumed to be equal to the pressure in the undisturbed atmosphere at the corresponding altitude. Buoyancy will cause the heated gas, initially at rest, to rise and bring into motion new layers of the atmosphere. This is accompanied by convective and diffusive mixing of the heated and cold air, which equalizes the temperature and density of the gas inside and outside the perturbed region [8, 9].

The motion of the air during ascent of the thermal is described by the complete system of Navier–Stokes equations for a viscous compressible heat-conducting gas. This system appears as follows in a cylindrical coordinate system written in matrix form for the dimensionless variables

$$\frac{\partial f}{\partial t} + Af = F, \quad A = A_1 + A_2 + A_3 + A_4, \tag{1}$$

where $f = \begin{pmatrix} \rho \\ u \\ v \\ T \end{pmatrix}$ is the vector of the unknown variables, while the differential matrix opera-

Moscow. Translated from Zhurnal Prikladnoi Mekhaniki i Tekhnicheskoi Fiziki, No. 3, pp. 78-81, May-June, 1985. Original article submitted March 30, 1984.

 0021-8944/85/2603-0370$09.50 © 1985 Plenum Publishing Corporation